

# Prediction of stiffness degradation in composite laminate with transverse cracking and delamination under hygrothermal conditions—desorption case

B. Boukert<sup>1a</sup>, M. Khodjet-Kesba<sup>\*1</sup>, A. Benkhedda<sup>1b</sup> and E.A. Adda Bedia<sup>2c</sup>

<sup>1</sup>Aeronautical Sciences Laboratory, Institute of Aeronautics and Space Studies, University of Blida 1,  
BP 270 Route de Soumaa, Blida 09000, Algeria

<sup>2</sup>Laboratory of Materials and Hydrology, University of Sidi Bel Abbes, Sidi Bel Abbes, Algeria

(Received December 16, 2023, Revised March 5, 2024, Accepted April 2, 2024)

**Abstract.** The stiffness reduction of cross-ply composite laminates featuring a transverse cracking and delamination within the mid-layer is predicted through utilization of a modified shear-lag model, incorporating a stress perturbation function. Good agreement is obtained by comparing the prediction models and experimental data. The material characteristics of the composite are affected by fluctuations in temperature and transient moisture concentration distribution in desorption case, based on a micro-mechanical model of laminates. The transient and non-uniform moisture concentration distribution induces a stiffness reduction. The obtained results demonstrate the stiffness degradation dependence on factors such as cracks density, thickness ratio and environmental conditions. The present study underscores the significance of comprehending the degradation of material properties in the failure progression of laminates, particularly in instances of extensive delamination growth.

**Keywords:** delamination; desorption; hygrothermal effect; stiffness; transverse cracking; Tsai model

## 1. Introduction

Typically, antecedent analyses solely focus on transverse cracking phenomena. However, a comparative investigation (Berthelot *et al.* 1996) juxtaposing empirical findings with outcomes derived from analytical models elucidates that transverse cracking merely constitutes one facet of the damage mechanism prevalent at elevated crack densities. Transverse fissures precipitate localized stress concentrations at the crack fronts, precipitating inter-laminar delamination between 0° and 90° layers. Delamination initiation stems from crack tip propagation and alleviates localized stress concentrations. In the context of composite structures, the emergence of delamination originating from transverse cracks is deemed a compelling rationale for removing the structure from operational duty. Therefore, a comprehensive examination of the ramifications of localized delamination originating and propagating from transverse crack tips is imperative.

---

\*Corresponding author, Ph.D., E-mail: mkhojet@gmail.com

<sup>a</sup>Ph.D., E-mail: bilanosky@hotmail.fr

<sup>b</sup>Professor, E-mail: aaminbenkhedda@gmail.com

<sup>c</sup>Professor, E-mail: addaded@yahoo.com

However, few studies have been conducted on the analysis of delamination induced by transverse cracks (Zhang *et al.* 2006, Van der Meer and Sluys 2013, Barbero *et al.* 2014, Zubillaga *et al.* 2015, Li 2016, Carraro *et al.* 2019).

Jayant *et al.* (2022) investigated the impact of delamination on the flutter performance of a smart laminated composite wing-like plate structure subjected to hygrothermal conditions. They developed a finite element model using Matlab for a laminated composite plate featuring a centrally located mid-plane square delamination and an actuator positioned at the top of the laminate. Additionally, an aerodynamic model was constructed in Nastran and linked with structural modal parameters using the surface spline technique. The study analyzed the influence of delamination size on aeroelastic performance under adverse levels of moisture and temperature. Results indicated a substantial deterioration in the plate's aeroelastic performance in the presence of delamination under adverse hygrothermal conditions. Moreover, there was observed an increase in structural stiffness alongside improvements in aeroelastic performance.

Yun-Tao (2022) conducted an experimental and numerical investigation into the hygrothermal effects on the mechanical behavior and failure mechanisms of single-lap countersunk-screwed joints between carbon fiber reinforced polyimide composite and metal. The study involved accelerated moisture absorption tests on plates until reaching effective moisture equilibrium, followed by quasi-static tension tests on single-lap countersunk-screwed joints made of CCF300/AC721-30CrMnSiA in different environmental conditions: room temperature and dry (RD), room temperature and wet (RW), and elevated temperature (+55°C) and wet (EW). Moisture and temperature impacts were analyzed, taking into account hygrothermal-mechanical interactions, with predictions closely aligning with experimental results. The findings suggest that delamination around the screw hole is likely the primary cause of final joint failure. Furthermore, the adverse hygrothermal effect on joint performance is primarily attributed to the degradation of inter-laminar properties of the composite laminate due to increased moisture and temperature levels.

Numerous experimental investigations have been conducted to assess the effects of hygrothermal aging on composite laminates, as evidenced by studies such as Deepa *et al.* (2016), Pereira Fulco *et al.* (2019), Singh and Angra (2019), Behera *et al.* (2020). In terms of analytical approaches, Adda Beddia *et al.* (2008), Khodjet-kesba *et al.* (2016, 2018) employ a comprehensive parabolic shear-lag model integrated with a micro-mechanical model, which considers variations in temperature and moisture concentration distributions to predict the influence of transverse cracks on stiffness degradation. Bouazza *et al.* (2007) derived a general expression for longitudinal modulus reduction concerning transverse cracks by introducing the stress perturbation function. These findings elucidate the intricate relationship between elastic property degradation and factors such as crack density, fiber orientation angle, and hygrothermal conditions.

Sheng *et al.* (2023) investigated the impact of hygrothermal aging on the interlaminar fracture characteristics of carbon fiber/epoxy composite laminates reinforced with core-shell rubber nanoparticles, micro-fiber non-woven thermoplastic veils, and a combination of nanoparticles and veils. They conducted double cantilever beam and end-notch flexure fracture tests under conditions of complete dryness, moisture saturation, and subsequent redrying of the laminates. The findings indicate significant alterations in the Mode-I and Mode-II fracture behaviors, including changes in R-curves, fracture energies, and crack propagation paths, for both baseline laminates and those toughened with nanoparticles and veils, due to hygrothermal aging.

Bahera *et al.* (2023) conducted an investigation into the phenomenon of interfacial debonding resulting from hygrothermal aging. They employed Field Emission Scanning Electron Microscopy and Atomic Force Microscopy to quantify this phenomenon on fiber/epoxy cross-ply laminate

coupons, which were then compared with unaged samples. Composite laminates aged for 1000 hours and 2000 hours were utilized to assess the extent of debonding. The results revealed that the interfacial debonding arc length of inner plies exceeded that of the respective outer plies by 14%, 17%, and 21%, respectively. Additionally, the variation in residual stress across inner plies was more pronounced compared to outer plies due to the latter's greater freedom of expansion.

Hanyu *et al.* (2023) investigated the combined effects of long-term hygrothermal aging and short-term temperature variations on the mechanical properties of Al/CFRP hybrid (riveted/bonded) joints. This study employed quasi-static tensile experiments along with advanced simulation methods. The experimental findings indicated that joint strength was primarily influenced by temperature variations, whereas breaking elongation showed sensitivity to the extent of aging. Furthermore, the joint stiffness and strength experienced a notable decrease under the simultaneous influence of temperature elevation and increased aging severity.

Oshin *et al.* (2023) conducted a comprehensive study on the low-velocity impact behavior of fiber-reinforced polymer composites due to their widespread applications across various domains. This investigation revealed a multitude of internal damages and intricate failure mechanisms, leading to a notable decline in the structural characteristics of the composites. Several factors were identified to influence the impact resistance and damage tolerance of these composites, including fabric architecture, resin toughness, environmental conditions, stacking sequence, and hybridization. Moreover, polymer composites utilized in outdoor applications are subjected to diverse hygrothermal conditions, resulting in moisture absorption and subsequent physiochemical changes within the matrix material, including plasticization, hydrolysis, and swelling. Prolonged exposure to such environments induces material property degradation, thereby compromising the overall performance and durability of the structures.

Jing *et al.* (2023) conducted an analysis on the impact of hygrothermal aging on the mechanical properties of fiber-metal-laminates (FMLs) featuring various innovative metal surface treatments. These treatments included nano-scale electrochemical sculpture. Specimens with differing edge conditions were fabricated using either milling or wire-electrode cutting methods and subsequently subjected to hygrothermal aging treatment within a climatic test chamber set at 60°C and 96% relative humidity. Results from interlaminar shear and flexural testing revealed distinct outcomes based on the machining method employed. Wire-electrode cutting resulted in edges with exposed fibers and resin spalling following hygrothermal aging, while milling cutting yielded edges characterized by a micro-porous and defective surface. The extent of reduction in interlaminar shear strength and flexural strength varied based on the specific surface treatments and machining methods utilized.

Li-Cai (2023) investigated the effects of both hygrothermal and thermal aging on adhesive bonding joints comprising similar and dissimilar specimens. The study focused on the single lap joint (SLJ) configuration, utilizing Aluminium/Aluminium and CFRP/CFRP for similar bonding, and Aluminium/CFRP for dissimilar bonding. The strength of the samples, subjected to no aging, hygrothermal aging, and thermal aging, was evaluated through three-point bending tests. Results indicated that the highest joint strength was observed in Aluminium/Aluminium bonds, with strength decreasing following both thermal and hygrothermal aging. Furthermore, the patterns of failure and the number of cycles leading to failure varied with load percentage and aging conditions.

Wen (2023) investigated the hygrothermal aging behaviour of E-glass fiber/epoxy composites. Moisture absorption data and diffusivity of the composite laminates were determined through five sets of aging tests conducted at varying temperatures and humidity. Utilizing the Shen and

Springer model along with the Arrhenius model, a relationship model was proposed between environmental parameters and moisture absorption behaviour. This model was validated using experimental data and Fick's law. Scanning electron microscopy observations revealed that swelling cracks and fiber/matrix interface debonding, induced by moisture absorption of the resin matrix, are the primary factors influencing the macroscopic properties of the composites.

This paper employs a modified shear lag model, incorporating parabolic analysis and progressive shear, to forecast the impact of transverse cracks and delamination on the stiffness degradation of transiently hygrothermal aged composite laminates. Good agreement is obtained by comparing prediction with experimental data. Subsequently, the cracked cross-ply composite laminates undergo initial exposure to hygrothermal aging, experiencing transient and non-uniform moisture concentration distribution during the desorption phase. To capture this phenomenon, Tsai model is employed, allowing for the introduction of aging and observation of its progression at both the fiber and matrix scales.

## 2. Theoretical analysis

In the absence of a unified theory for the mechanical characterization of composite materials with long fibers, several formulations have been proposed in the literature. These include the rule of mixtures method, the contiguity method which relies on fiber arrangement (Staab 1999, Maurice 2001), the semi-empirical approach based on Halpin-Tsai theory (Halpin and Tsai 1968), and the additional technique method based on fiber placement (Chamis 1983).

In this paper, we applied the rule of mixtures method to analyze composites with anisotropic fibers, a modification introduced by Hahn as described in Reference (Tsai 1988). Consequently, the longitudinal Young's modulus for a unidirectional composite is calculated as follows

$$E_x = E_m \cdot V_m + E_{fx} \cdot V_f \quad (1)$$

The modified micromechanics method for calculating the transverse modulus of a graphite/epoxy (T300/5208) composite is determined as follows

$$E_y = \frac{1+0.516(V_m/V_f)}{\frac{1}{E_{fy}} + \frac{0.516(V_m/V_f)}{E_m}} \quad (2)$$

In a similar manner, the shear modulus and Poisson's ratio can be determined as follows

$$G_{xy} = \frac{1+0.316(V_m/V_f)}{\frac{1}{G_{fx}} + \frac{0.316(V_m/V_f)}{G_m}} \quad (3)$$

$$\nu_{xy} = V_f \nu_f + V_m \nu_m \quad (4)$$

In the above equations,  $V_f$  and  $V_m$  represent the fiber and matrix volume fractions, respectively, and they are related by

$$V_f + V_m = 1 \quad (5)$$

$E_f$ ,  $G_f$ , and  $\nu_f$  are the Young's modulus, shear modulus, and Poisson's ratio, respectively, of the fiber, while  $E_m$ ,  $G_m$ , and  $\nu_m$  are the corresponding properties for the matrix.

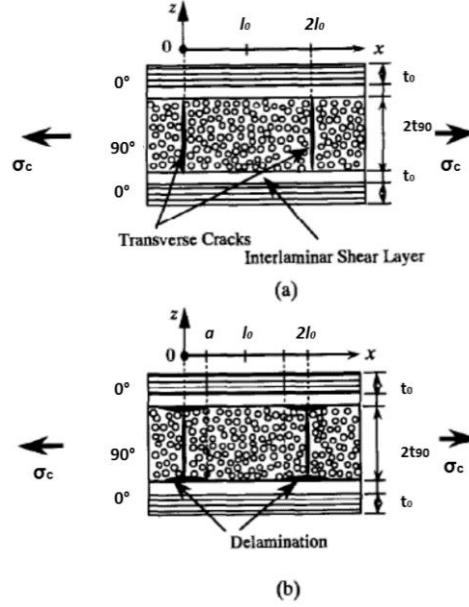


Fig. 1 Cross-ply composite laminates: (a) with transverse cracks; (b) with transverse cracks and delamination

## 2.1 Stiffness reduction model

We consider a symmetric  $[0/90]_s$  laminate subjected to uniaxial loads. It is assumed that the 90° ply has developed continuous intra-laminar cracks and that a delamination with a length of  $2a$  has formed at each tip of the transverse cracks (with a crack spacing of  $2l_0$ ) as shown in (Fig. 1).

Loading is applied only in x-direction and the far field applied stress is defined by  $\sigma_c = (1/2h)N_x$ , where  $N_x$  is the applied load. The subsequent analysis will be conducted under the assumption of a generalized plane strain condition.

$$\varepsilon_y^\theta = \varepsilon_y^{90} = \varepsilon_y = \text{const} \quad (6)$$

The symbol ( $\bar{\quad}$ ) over stress and strain components denotes volume average. They are calculated using the following expressions

- In the 0° layer.

$$\bar{f}^0 = \frac{1}{2l_0} \frac{1}{t_0} \int_{-l_0}^{+l_0} \int_{t_{90}}^h f^0 dx dz = \frac{1}{2l_0} \frac{1}{\alpha} \int_{-l_0}^{+l_0} \int_1^{\bar{h}} f^0(\bar{x}, \bar{z}) d\bar{x} d\bar{z} \quad (7)$$

- In the 90° layer.

$$\bar{f}^{90} = \frac{1}{2l_0} \frac{1}{t_{90}} \int_{-l_0}^{+l_0} \int_0^{t_{90}} f^{90} dx dz = \frac{1}{2l_0} \frac{1}{\alpha} \int_{-l_0}^{+l_0} \int_0^1 f^{90}(\bar{x}, \bar{z}) d\bar{x} d\bar{z} \quad (8)$$

By utilizing the strains in the 0° layer (which is not damaged and, hence, strains are equal to laminate strains,  $\varepsilon_x = \bar{\varepsilon}_x^0$ , etc.) and assuming zero residual stresses, the Young's modulus of the laminate with cracks is defined by the following expression

$$E_x = \frac{\sigma_c}{\bar{\varepsilon}_x^0} \quad (9)$$

Note that the initial laminate modulus measured at the same load is  $E_{x0} = \frac{\sigma_c}{\varepsilon_{x0}}$  and, hence

$$\frac{E_x}{E_{x0}} = \frac{\varepsilon_{x0}}{\bar{\varepsilon}_x^0} \quad (10)$$

## 2.2 Stress and strain perturbation caused by transverse cracks

The constitutive equations that establish the relationship between strain and stresses are as follow:

- In the 90° layer.

$$\begin{Bmatrix} \varepsilon_x^{90} \\ \varepsilon_y^{90} \\ \varepsilon_z^{90} \end{Bmatrix} = \begin{bmatrix} S_{22} & S_{12} & S_{23} \\ S_{12} & S_{11} & S_{12} \\ S_{32} & S_{12} & S_{22} \end{bmatrix} \begin{Bmatrix} \sigma_x^{90} \\ \sigma_y^{90} \\ \sigma_z^{90} \end{Bmatrix} \quad (11)$$

- In the 0° layer.

$$\begin{Bmatrix} \varepsilon_x^0 \\ \varepsilon_y^0 \\ \varepsilon_z^0 \end{Bmatrix} = \begin{bmatrix} S_{11} & S_{12} & S_{13} \\ S_{12} & S_{22} & S_{23} \\ S_{13} & S_{23} & S_{33} \end{bmatrix} \begin{Bmatrix} \sigma_x^0 \\ \sigma_y^0 \\ \sigma_z^0 \end{Bmatrix} \quad (12)$$

Where  $S_{ij}$  is the compliance matrix for a unidirectional composite with a 0° fiber orientation. To compute the laminate elastic property, we require  $\bar{\varepsilon}_x^0$ . By averaging Eqs. (8) and (9), we obtain the averaged constitutive equations for the 90° and 0° layers. In these averaged relationships, we have  $\bar{\sigma}_z^{90} = \bar{\sigma}_z^0 = 0$ , which follows from force equilibrium in the  $z$ -direction

$$\int_{-l_0}^{+l_0} \sigma_z^i dx = 0, \quad i = 90, 0 \quad (13)$$

The averaged constitutive equations corresponding to in-plane normal stress and strain components are as follows

$$\begin{Bmatrix} \bar{\varepsilon}_x^0 \\ \bar{\varepsilon}_y^0 \end{Bmatrix} = \begin{bmatrix} S_{11} & S_{12} \\ S_{12} & S_{22} \end{bmatrix} \begin{Bmatrix} \bar{\sigma}_x^0 \\ \bar{\sigma}_y^0 \end{Bmatrix} \quad (14)$$

$$\begin{Bmatrix} \bar{\varepsilon}_x^{90} \\ \bar{\varepsilon}_y^{90} \end{Bmatrix} = \begin{bmatrix} S_{22} & S_{12} \\ S_{12} & S_{11} \end{bmatrix} \begin{Bmatrix} \bar{\sigma}_x^{90} \\ \bar{\sigma}_y^{90} \end{Bmatrix} \quad (15)$$

Eqs. (14) and (15) are obtained from the 3D strain-stress relationships, yet due to Eq. (13), the outcome resembles that of classical thin-laminate theory (CLT). In fact, for an undamaged laminate, the averaged stresses and strains are equal to the laminate theory stresses and strains and Eqs. (14) and (15) are still applicable.

Force equilibrium equations for a damaged (or undamaged) laminate are:

- In  $x$ -direction

$$N_x = \int_0^{t_{90}} \sigma_x^{90} dz + \int_{t_{90}}^h \sigma_x^0 dz = \sigma_c(t_{90} + t_0) \quad (16)$$

Leading to

$$\bar{\sigma}_x^{90} t_{90} + \bar{\sigma}_x^0 t_0 = \sigma_c(t_{90} + t_0) \quad (17)$$

- In  $y$ -direction

$$N_y = 0 \implies \int_0^{t_{90}} \sigma_y^{90} dz + \int_{t_{90}}^h \sigma_y^0 dz = 0 \quad (18)$$

From which follows

$$\bar{\sigma}_y^{90} t_{90} + \bar{\sigma}_y^0 t_0 = 0 \quad (19)$$

Eqs. (14), (15), (17), and (19) involve seven unknowns: four stress components and three strain components ( $\bar{\varepsilon}_x^{90}$ ,  $\bar{\varepsilon}_x^0$  and  $\varepsilon_y$ ). However, the total number of equations is six. Therefore, one of the unknowns can be considered as independent, and the remaining ones can be expressed as linear functions of it. By selecting the stress  $\bar{\sigma}_x^{90}$  as independent and solving the system of Eqs. (14), (15), (17), and (19) with respect to it, we obtain

$$\varepsilon_y = g_1 \bar{\sigma}_x^{90} + f_1 \sigma_c, \bar{\varepsilon}_x^{90} = g_2 \bar{\sigma}_x^{90} + f_2 \sigma_c, \bar{\varepsilon}_x^0 = g_3 \bar{\sigma}_x^{90} + f_3 \sigma_c \quad (20)$$

Expressions for  $g_i, f_i, i=1,2,3$  through laminate geometry and properties of constituents are given as follows

$$g_1 = t_{90} \frac{S_{12}S_{22} - S_{11}S_{12}}{S_{11}t_0 + S_{22}t_{90}}, f_1 = \frac{S_{11}S_{12}(t_0 + t_{90})}{S_{11}t_0 + S_{22}t_{90}} \quad (21)$$

$$g_2 = S_{22} - \frac{S_{12}(S_{12}t_0 + S_{12}t_{90})}{S_{11}t_0 + S_{22}t_{90}}, f_2 = \frac{S_{12}S_{12}(t_0 + t_{90})}{S_{11}t_0 + S_{22}t_{90}} \quad (22)$$

$$g_3 = \frac{t_{90}}{t_0} \left( S_{12} \frac{(S_{12}t_0 + S_{12}t_{90})}{S_{11}t_0 + S_{22}t_{90}} - S_{11} \right), f_3 = \frac{t_0 + t_{90}}{t_0} \left( S_{11} - \frac{(S_{12})^2 t_{90}}{S_{11}t_0 + S_{22}t_{90}} \right) \quad (23)$$

In order to obtain an expression for average stress  $\bar{\sigma}_x^{90}$  in the repeatable unit, we consider the axial stress perturbation induced by the presence of two cracks. Without losing generality the axial stress distribution may be written in the following form

$$\sigma_x^{90} = \sigma_{x0}^{90} - \sigma_{x0}^{90} f_1(\bar{x}, \bar{z}) \quad (24)$$

$$\sigma_x^0 = \sigma_{x0}^0 + \sigma_{x0}^0 f_2(\bar{x}, \bar{z}) \quad (25)$$

Where  $\sigma_{x0}^{90}$  is the CLT stress in the 90° layer and  $\sigma_{x0}^0$  is the CLT stress in the 0° layer (laminate theory routine),  $-\sigma_{x0}^{90} f_1(\bar{x}, \bar{z})$  and  $\sigma_{x0}^0 f_2(\bar{x}, \bar{z})$  represent stress perturbation caused by the presence of cracks. Normalising factors in form of far field stresses in perturbation functions are used for convenience. By averaging Eqs. (24) and (25) using the integral force equilibrium in the  $x$ -direction (Eq. (16)), we obtain

$$\bar{\sigma}_x^{90} = \sigma_{x0}^{90} - \sigma_{x0}^{90} \frac{1}{2\bar{l}_0} R(\bar{l}_0) \quad (26)$$

$$\bar{\sigma}_x^0 = \sigma_{x0}^0 + \sigma_{x0}^0 \frac{1}{2\alpha\bar{l}_0} R(\bar{l}_0) \quad (27)$$

In the following function

$$R(\bar{l}_0) = \int_{-\bar{l}_0}^{+\bar{l}_0} \int_0^1 f_1(\bar{x}, \bar{z}) d\bar{z} d\bar{x} \quad (28)$$

$R(\bar{l}_0)$  is referred to stress perturbation function. It's related to axial stress perturbation in the 90° layer and depends on the crack density.

The average stress  $\bar{\sigma}_x^{90}$  involved in Eq. (20) is now expressed through the stress perturbation function Eq. (28). The conditions used to obtain expressions (Eq. (20)) are identical to those used in CLT. Hence, substituting  $\bar{\sigma}_x^{90} = \sigma_{x0}^{90}$  where  $\sigma_{x0}^{90}$  is the  $x$ -axis stress in the 90° layer according to

CLT, we obtain CLT solution:  $\bar{\varepsilon}_x^{90} = \varepsilon_{x0}^{90} = \varepsilon_{x0}$ ,  $\bar{\varepsilon}_x^0 = \varepsilon_{x0}^0 = \varepsilon_{x0}$  and  $\varepsilon_y = \varepsilon_{y0}$ .

Substituting Eq. (26), which comprises two terms, into Eq. (20), the resulting expression contains two terms. The first term, as discussed earlier, is equivalent to the CLT strain, but the second term introduces a new component associated with the stress perturbation function ( $\bar{l}_0$ )

$$\varepsilon_y = \varepsilon_{y0} - \sigma_{x0}^{90} g_1 \frac{1}{2\bar{l}_0} R(\bar{l}_0) \quad (29)$$

$$\bar{\varepsilon}_x^{90} = \varepsilon_{x0} - \sigma_{x0}^{90} g_2 \frac{1}{2\bar{l}_0} R(\bar{l}_0) \quad (30)$$

$$\bar{\varepsilon}_x^0 = \varepsilon_{x0} - \sigma_{x0}^{90} g_3 \frac{1}{2\bar{l}_0} R(\bar{l}_0) \quad (31)$$

The stress  $\sigma_{x0}^{90}$  in the 90° layer of an undamaged laminate under mechanical loading may be calculated using CLT

$$\sigma_{x0}^{90} = Q_{22} \varepsilon_{x0} (1 - \nu_{12} \nu_{xy}^0) \quad (32)$$

Here,  $\nu_{xy}^0$  is the Poisson's ratio of the undamaged laminate.

### 2.3 Stress and strain perturbation caused by transverse cracks and delamination

In the delamination damage range,  $l-a \leq x \leq l$ , the 90° layer cannot bear any load due to the presence of transverse cracks. Therefore, we have

$$\overline{\sigma_{xx}^0} = \frac{t_0 + t_{90}}{t_0} \overline{\sigma_c} \quad (33)$$

$$\overline{\sigma_{xx}^{90}} = 0 \quad (34)$$

$t_0$  and  $t_{90}$  represent the thickness of 0° layer and 90° layer respectively,  $\overline{\sigma_c}$  is the average stress.

However, in the non-delaminated range,  $0 \leq x \leq l-a$ , both the 0° and 90° layer bear the load jointly. The stress of the 0° layer is determined as

$$\overline{\sigma_{xx}^0} = \overline{\sigma_c} \frac{E_0}{E_{x0}} \left[ 1 + \frac{t_{90} E_{90}}{t_0 E_0} \frac{\cosh(\xi \bar{l}_0 \frac{x}{\bar{l}_0})}{\cosh(\xi \bar{l}_0)} \right] \quad (35)$$

The 90°-layer stress is

$$\overline{\sigma_{xx}^{90}} = \overline{\sigma_c} \frac{E_0}{E_{x0}} \left[ 1 - \frac{\cosh(\xi \bar{l}_0 \frac{x}{\bar{l}_0})}{\cosh(\xi \bar{l}_0)} \right] \quad (36)$$

Where  $\xi$  is the shear-lag parameter.

Since the longitudinal strains in the delaminated range and non-delaminated range are different. We compute the longitudinal average strain as follow

$$\begin{aligned} \varepsilon_c &\approx \bar{\varepsilon}_x^0 = \frac{1}{l_0} \int_0^{l_0} \frac{\overline{\sigma_{xx}^0}}{E_0} dx \\ &= \frac{1}{l_0} \int_{l_0-a}^{l_0} \frac{t_0 + t_{90}}{E_0 t_0} \overline{\sigma_c} dx + \frac{1}{l_0} \int_{l_0-a}^{l_0} \frac{\overline{\sigma_c}}{E_{x0}} \left( 1 + \frac{t_{90} E_{90} \cosh(\xi \bar{l}_0 \frac{x}{\bar{l}_0})}{t_0 E_0 \cosh(\xi \bar{l}_0)} \right) dx \\ &= \frac{a}{l_0} \frac{t_0 + t_{90}}{E_0 t_0} \overline{\sigma_c} + \frac{l_0 - a}{l_0} \frac{\overline{\sigma_c}}{E_{x0}} + \frac{t_{90} E_{90}}{t_0 E_0 E_{x0} \cosh(\xi \bar{l}_0)} \frac{\overline{\sigma_c}}{\xi \bar{l}_0} \sinh\left(\xi \bar{l}_0 \left(1 - \frac{a}{l_0}\right)\right) \end{aligned} \quad (37)$$

Defining  $n$  as the delamination propagation rate,  $a$  represents half of the delaminated crack

length.

#### 2.4 Expression for elastic constant

In order to derive an expression for the longitudinal modulus  $E_x$  of the damaged laminate with only transverse cracks, we utilize the definition in Eq. (10) and substitute Eq. (31) in this relationship. Finally, we employ Eq. (32). This procedure yields

$$\frac{E_x}{E_{x0}} = \frac{1}{1+b\bar{\rho}R(\bar{l}_0)} \quad (38)$$

Where  $\bar{\rho} = \frac{1}{2\bar{l}_0}$ ,  $\bar{l}_0 = \frac{l_0}{t_{90}}$  is the normalized crack density and  $a$ ,  $b$  are known functions, dependent on elastic properties and geometry of the  $0^\circ$  and  $90^\circ$  layer

$$b = \frac{E_{90}t_{90}}{E_x^0t_0} \left( \frac{1-\nu_{12}\nu_{xy}^0}{1-\nu_{12}\nu_{21}} \right) \left( 1 + \nu_{xy}^0 \frac{S_{12}t_{90}+S_{12}t_0}{S_{22}t_0+S_{11}t_0} \right) \quad (39)$$

$E_x^0$  and  $E_{90}$  are the Young's modulus of  $0^\circ$  and  $90^\circ$  layers respectively.

From Eqs. (35) and (37) and also  $\sigma_c = E_x \varepsilon_c$ ,  $a = nl_0$  and  $l_0 = \frac{1}{2\rho}$ , the longitudinal modulus  $E_x$  of the damaged laminate with transverse cracks and delamination can be obtained

$$\frac{E_x}{E_{x0}} = \frac{1}{E_{x0} \left( n \frac{t_0+t_{90}}{E_0t_0} + \frac{1-n}{E_{x0}} + \frac{t_{90}E_{90} \left[ \frac{2\rho}{n\xi} \sinh \left( \frac{(1-n)\xi}{2\rho} \right) \right]}{t_0E_0E_{x0} \cosh \left( \frac{n\xi}{2\rho} \right)} \right)} \quad (40)$$

From Eqs. (38) and (40), it is evident that the functions  $R(\bar{l}_0)$  and  $\xi$  are the only unknowns. Consequently, the reduction of the Young's modulus depends on the form of this function of crack density. Solutions for these functions can be determined using various analytical models such as shear-lag models.

#### 2.5 Computation of stress perturbation function using shear lag model

In this study, two models developed by Berthelot *et al.* (1996) have been employed. The latter is modified by introducing the stress perturbation function. The stress perturbation function  $R(\bar{l}_0)$  is determined as

$$R(a) = \int_{-\bar{l}_0}^{+\bar{l}_0} \frac{\cosh(\xi\bar{x})}{\cosh(\xi\bar{l}_0)} d\bar{x} = \frac{2}{\xi} \tanh(\xi\bar{l}_0) \quad (41)$$

Where

$$\xi^2 = \bar{G} \frac{t_{90}(t_{90}E_{90}+t_{\theta}E_{\theta})}{t_{\theta}E_{90}E_{\theta}} \quad (42)$$

The coefficient  $\bar{G}$  depends on the assumptions made regarding the longitudinal displacement and shear stress distribution:

- In the first case, it is assumed that the longitudinal displacement is parabolic across the thickness of the  $90^\circ$  layer

$$u_{90}(x, z) = \bar{u}_{90}(x) + \left( z^2 - \frac{t_{90}^2}{3} \right) A_{90}(x) \quad (43)$$

The variation of the longitudinal displacement is to be determined by the thickness of  $\theta^\circ$  layers

$$u_0(x, z) = \bar{u}_0(x) + f(z)A_0(x) \quad (44)$$

• In the second case, it is assumed that the shear stresses, which are similar in the  $0^\circ$  and  $90^\circ$  layers, can be obtained by assuming that the transverse displacement is independent of the longitudinal coordinate

$$\sigma_{xz}^i = G_{xz}^i \gamma_{xz}^i \quad (45)$$

$$\gamma_{xz}^i = \frac{\partial u_i}{\partial z} + \frac{\partial w_i}{\partial x} \approx \frac{\partial u_i}{\partial z} \quad i = 0^\circ, 90^\circ \quad (46)$$

The coefficient  $\bar{G}$  is given as follow

$$\bar{G} = \frac{3G}{t_{90}} \quad (47)$$

The shear modulus  $G$  of the elementary cell

$$G = \frac{G_{xz}^{90}}{1 - 3 \frac{G_{xz}^{90}}{G_{xz}^0} \frac{f(t_{90})}{f'(t_{90})}} \quad (48)$$

Two distinct analytical functions for the variation function have been considered (Berthelot *et al.* 1996):

• In the case of the assumption of parabolic variation of longitudinal displacement in both  $0^\circ$  and  $90^\circ$  layers, by replacing the function  $f(z) = z^2 - 2(t_0 + t_{90})z + \frac{2}{3}t_0^2 + 2t_0t_{90} + t_{90}^2$  in the Eq. (48), the shear modulus for parabolic assumption will be

$$G = \frac{G_{xz}^{90}}{1 + \alpha \frac{G_{xz}^{90}}{G_{xz}^0}} \quad (49)$$

• In the case where longitudinal displacement is assumed to be progressive in the  $0^\circ$  layer, we use the function  $f(z) = \frac{\sinh \alpha \eta_t}{\alpha \eta_t} - \cosh \eta_t (1 + \alpha - \frac{z}{t_{90}})$  in Eq. (48), the shear modulus for progressive shear assumption will be

$$G = \frac{G_{xz}^{90}}{1 + 3\alpha \frac{\alpha \eta_t (\tanh \alpha \eta_t)^{-1} - 1}{\alpha \eta_t^2} \frac{G_{xz}^{90}}{G_{xz}^0}} \quad (50)$$

$\eta_t$  is the shear transfer parameter.

## 2.6 Influence of transient hygrothermal conditions on stiffness reduction

This study focuses on the stiffness reduction resulting from transverse cracking and delamination in a  $[0/90_3]_s$  composite laminate when exposed to hygrothermal conditions initially. The Tsai model (1988) is employed as the model enabling the introduction of aging and observation of its development on both fiber and matrix scales. The principle of this simplified method involves considering the actual distribution of moisture concentration through each ply using its serial expansion (Vergnaud 1992). This facilitates the determination of the precise expression of stiffness under hygrothermal effects.

Tsai (1988) proposes an adimensional temperature  $T^*$ , which serves as the key parameter for assessing the hygrothermal effect on stress distribution

Table 1 Fibre and matrix characteristics of graphite/epoxy material (T300/5208) (Tsai 1988) ( $T=22^\circ\text{C}$  and  $C=0.5\%$ )

$E_{fx}^0$ (Gpa)	$E_{fy}^0$ (Gpa)	$E_m^0$ (Gpa)	$\nu_{fx}^0$	$\nu_m^0$	$G_{fx}^0$ (Gpa)	$G_m^0$ (Gpa)	$V_f$
259	18.69	3.4	0.25	0.35	19.69	1.26	0.7

Table 2 Parameters of temperature and moisture characteristics variation (Tsai 1988)

$T_g^0$ ( $^\circ\text{C}$ )	$T_{room}$ ( $^\circ\text{C}$ )	$g$ ( $^\circ\text{C}/c$ )	$d$	$f$
160	22	2000	0.35	0.04

$$T^* = \frac{T_g - T_{opr}}{T_g - T_{rm}} \quad (51)$$

Where  $T_g$  is the glass transition temperature,  $T_{opr}$  is the operating temperature and  $T_{rm}$  is the room temperature. Additionally, we assume that moisture suppresses the glass transition temperature  $T_g^0$  by a simple temperature shift.

$$T_g = T_g^0 - g \cdot c \quad (52)$$

Where  $T_g^0$  is the glass transition temperature at dry state,  $g$  is the temperature shift per unit of moisture absorbed and  $c$  is the absorbed moisture. The exponents of  $T^*$  can be utilized to empirically fit the matrix mechanical properties as a function of moisture and temperature.

$$\frac{E_m}{E_m^0} = \frac{G_m}{G_m^0} = \frac{\nu_m}{\nu_m^0} = (T^*)^d \quad (53)$$

$E_m^0$ ,  $G_m^0$  and  $\nu_m^0$  are the Young's modulus, shear modulus and Poisson's ratio, respectively, of the matrix at room temperature and  $d$  is an empirical constant. The same exponents of  $T^*$  is used to empirically fit the fiber mechanical properties as function of moisture and temperature.

$$\frac{E_{fx}}{E_{fx}^0} = \frac{E_{fy}}{E_{fy}^0} = \frac{G_{fx}}{G_{fx}^0} = \frac{\nu_{fx}}{\nu_{fx}^0} = (T^*)^f \quad (54)$$

$E_{fx}^0$ ,  $E_{fy}^0$ ,  $G_{fx}^0$  and  $\nu_{fx}^0$  are the longitudinal and transversal Young's modulus, shear modulus and Poisson's ratio, respectively, of the fiber at room temperature and  $f$  is an empirical constant.

It is assumed that  $E_m$ ,  $G_m$ ,  $\nu_m$ ,  $E_{fx}$ ,  $E_{fy}$ ,  $G_{fx}$  and  $\nu_{fx}$  are function of temperature and moisture (as Eqs. (53) and (54)), then  $E_x$ ,  $E_y$  and  $G_{xy}$  (as Eqs. (1), (2) and (3)) will be also function of temperature and moisture. In Tables 1 and 2, we identified the parameters that influence the mechanical characteristics of graphite/epoxy material.

Let's consider a laminated plate of thickness  $h$  made of polymer matrix composite, subjected on both sides to the same dry environment. The plate is assumed to be infinite in both  $x$  and  $y$  directions, and moisture only varies in the  $z$  direction. The initial moisture concentration  $C_{init}$  is uniform at  $t=0$ . Both sides of the plate are suddenly exposed to a zero-moisture environment (see Fig. 2). The moisture concentration inside the plate is described by Fick equation (Shen and Springer 1981, Benkhedda *et al.* 2008, Tounsi *et al.* 2005) with a diffusivity  $D_z$ .

$$\frac{\partial C}{\partial t} = D_z \frac{\partial^2 C}{\partial z^2} \quad (55)$$

The moisture diffusion characteristics are given in Table 3.

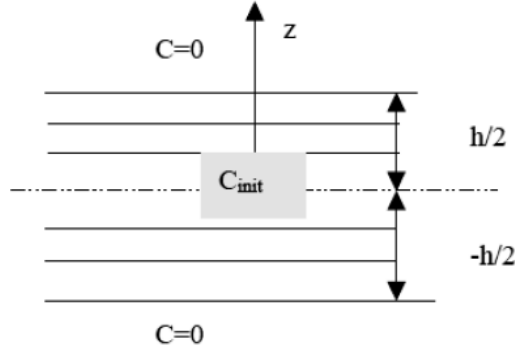


Fig. 2 Desorption phase

Table 3 Moisture diffusion characteristics (Tsai 1988)

Diffusivity, mm <sup>2</sup> /s	$D_z = 0.57 \exp(-4993/T)$ $T$ : Temperature (K)
Moisture concentration at the surface as a function of relative humidity, %	$C_{ini} = 0.015 \cdot H$ $H$ : Relative humidity (%)

With the initial conditions

$$C = C_{init} \text{ for } -h/2 \leq z \leq h/2 \text{ and } t = 0 \quad (56)$$

$$C = 0 \text{ for } z = -h/2 ; z = h/2 \text{ and } t > 0 \quad (57)$$

The initial conditions being uniform and boundary conditions are constants, the unidimensional solution of Fick equation can be expressed as (Benkhedda *et al.* 2008, Rezoug *et al.* 2011)

$$C(z, t) = \left[ \frac{4C_{ini}}{\pi} \sum_{n=0}^{\infty} \frac{(-1)^n}{(2n+1)} \cos\left(\frac{(2n+1)\pi z_k}{h}\right) \exp\left(\frac{-D_z(2n+1)^2 \pi^2 t}{h^2}\right) \right] \quad (58)$$

### 2.6.1 Relative stiffness reduction

Time  $t$  being given, the first step is to compute the on-axis free expansions  $E_x$ ,  $E_y$ ,  $G_{xy}$  and  $v_{xy}$ . These expansions are computed at each point  $z_k$  of thickness. Finally, the stiffness degradation in  $[0/90_3]_s$  composite laminate due to crack density with only transverse cracks and with both transverse cracks and delamination is evaluated, compared to the initial stiffness of the same uncracked laminate under the same environmental conditions. It should be noted that this initial stiffness of the uncracked laminate is a function of temperature and moisture distribution. Consequently, Eqs. (38) and (40) become:

a) For a laminate with only transverse cracks

$$\frac{E_{x(i)}}{E_{x0(i)}} = \frac{1}{1 + b_{(i)} \bar{\rho} R_{(i)}(\bar{l}_0)} \quad (59)$$

b) For a laminate with transverse cracks and delamination

$$\frac{E_{x(i)}}{E_{x0(i)}} = \frac{1}{E_{x0(i)} \left( n \frac{t_0 + t_{90}}{E_{0(i)} t_0} + \frac{1-n}{E_{x0(i)}} + \frac{t_{90} E_{90(i)} \left[ \frac{2\rho}{n \xi(i)} \sinh\left(\frac{(1-n)\xi(i)}{2\rho}\right) \right]}{t_0 E_{0(i)} E_{x0(i)} \cosh\left(\frac{n\xi(i)}{2\rho}\right)} \right)} \quad (60)$$

Table 4 Material properties of T800H/3631 laminate used in calculations (Takeda and Ogihara 1994)

T800H/3631	Room temperature (RT)	80°C
$E_0$ (GPa)	152.2	144.2
$E_{90}$ (GPa)	9.57	8.09
$G_0$ (GPa)	4.5	4.26
$G_{90}$ (GPa)	3.21	2.75
$\nu_0$	0.349	0.349
$\nu_{90}$	0.490	0.490

The index ( $i$ ) represents the considered case of environmental conditions.

### 2.6.2 Total stiffness reduction

In this section, the total stiffness reduction modulus is determined compared to the axial modulus of the uncracked laminate when it is initially exposed to environmental condition case 1. Consequently, this total stiffness reduction takes into account the reduction due to the crack density, moisture and temperature variation. Eqs. (38) and (40) become:

a) For a laminate with only transverse cracks

$$\frac{E_{x(i)}}{E_{x0(1)}} = \frac{(t_0 E_{0(i)} + t_{90} E_{90(i)})}{(1 + b_{(i)} \bar{\rho} R_{(i)}(l_0))(t_0 E_{0(1)} + t_{90} E_{90(1)})} \quad (61)$$

b) For a laminate with transverse cracks and delamination

$$\frac{E_{x(i)}}{E_{x0(1)}} = \frac{(t_0 E_{0(i)} + t_{90} E_{90(i)})}{E_{x0(i)} \left( n \frac{t_0 + t_{90}}{E_{0(i)} t_0 + E_{x0(i)}} + \frac{1-n}{E_{x0(i)}} + \frac{t_{90} E_{90(i)} \left[ \frac{2\rho}{n\xi(i)} \sinh\left(\frac{(1-n)\xi(i)}{2\rho}\right) \right]}{t_0 E_{0(i)} E_{x0(i)} \cosh\left(\frac{n\xi(i)}{2\rho}\right)} \right)} (t_0 E_{0(1)} + t_{90} E_{90(1)}) \quad (62)$$

## 3. Results and discussion

A computer code based on the preceding equations was developed to compute the stiffness loss for cross-ply laminates due to transverse ply cracking and delamination.

### 3.1 Comparison of predictions with experimental data

In this section, we will validate the present program results without considering the hygrothermal effect on the material properties. The results will be compared with experimental data for T800H/3631 laminates with elastic properties as shown in Table 4 (Takeda and Ogihara 1994). The thickness of each ply is approximately 0.132 mm, and the fiber volume fraction is about 0.6.

The degradation in longitudinal Young's modulus as a function of crack density for T800/3631  $[0/90_m]_s$  ( $m=2,4,6$ ) laminates at room temperature and at 80°C are depicted in Figs. 3-8. The results illustrate that the stiffness loss in  $[0/90_6]_s$  laminates (Figs. 5 and 8) is more significant than in  $[0/90_2]_s$  and  $[0/90_4]_s$  laminates. This is attributed to the fact that the 90° layers bear a larger portion

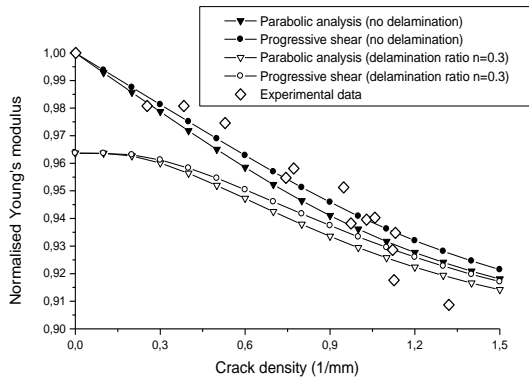


Fig. 3 Young's modulus reduction as function of crack density for T800H/3631 [0/90<sub>2</sub>]<sub>s</sub> laminate at room temperature

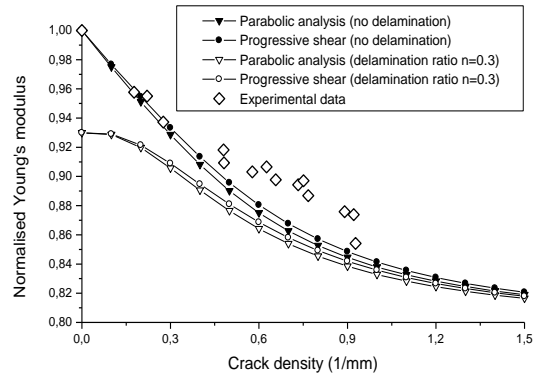


Fig. 4 Young's modulus reduction as function of crack density for T800H/3631 [0/90<sub>4</sub>]<sub>s</sub> laminate at room temperature.

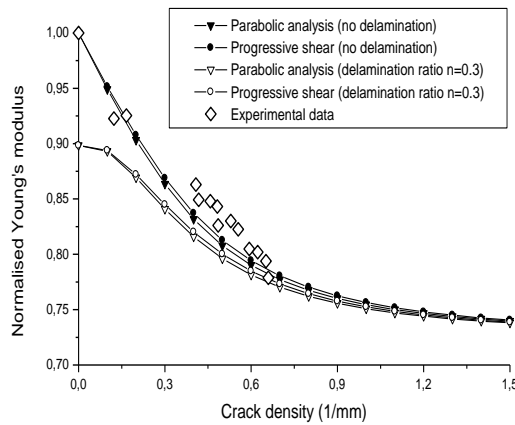


Fig. 5 Young's modulus reduction as function of crack density for T800H/3631 [0/90<sub>6</sub>]<sub>s</sub> laminate at room temperature

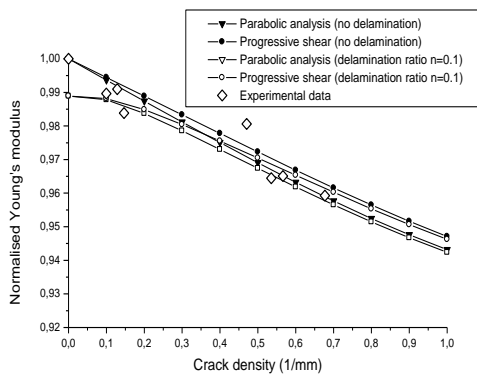


Fig. 6 Young's modulus reduction as function of crack density for T800H/3631 [0/90<sub>2</sub>]<sub>s</sub> laminate at 80°C

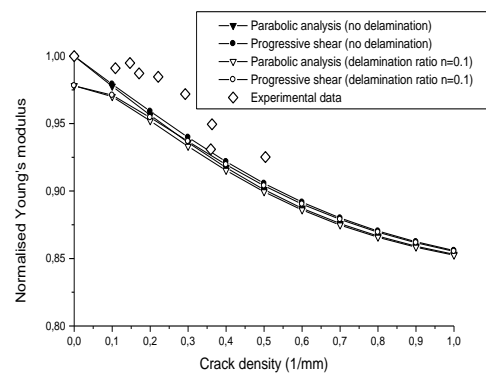


Fig. 7 Young's modulus reduction as function of crack density for T800H/3631 [0/90<sub>4</sub>]<sub>s</sub> laminate at 80°C

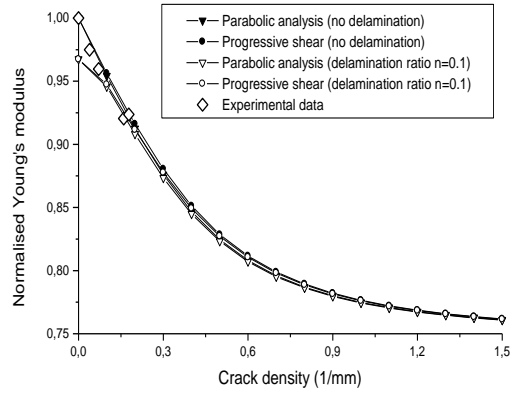


Fig. 8 Young's modulus reduction as function of crack density for T800H/3631  $[0/90_6]_s$  laminate at  $80^\circ\text{C}$

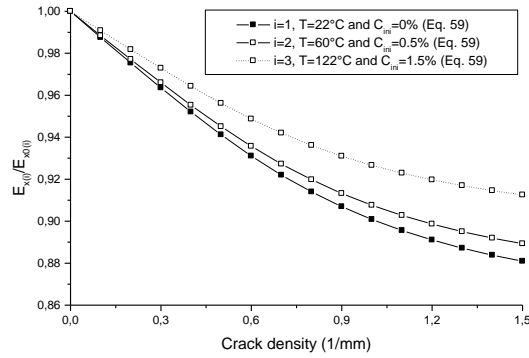


Fig. 9 Hygrothermal effect on the relative stiffness degradation due to: (Eq. (59)) transverse cracks only in a  $[0/90_3]_s$  graphite/epoxy (T300/5208)

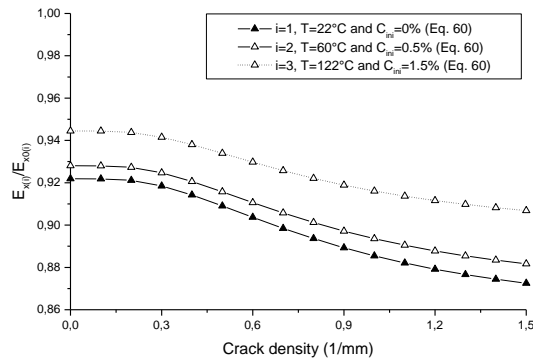


Fig. 10 Hygrothermal effect on the relative stiffness degradation due to: (Eq. (60)) transverse cracks and delamination in a  $[0/90_3]_s$  graphite/epoxy (T300/5208)

of the applied load due to their greater thickness in the uncracked  $[0/90_6]_s$  laminates. As a result, local delamination leads to a more pronounced loss in load carrying capacity for the  $[0/90_6]_s$  laminates. Therefore, the thickness ratio plays an important role in the residual stiffness for

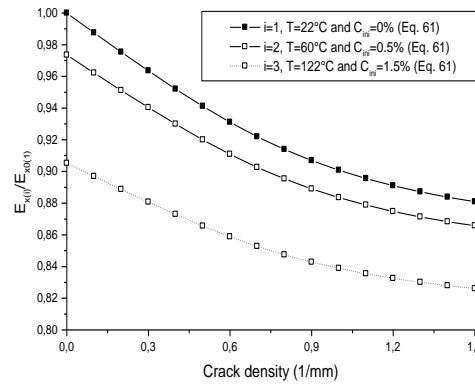


Fig. 11 Hygrothermal effect on the total stiffness degradation due to: (Eq. (61)) transverse cracks only in a  $[0/90_3]_s$  graphite/epoxy (T300/5208)

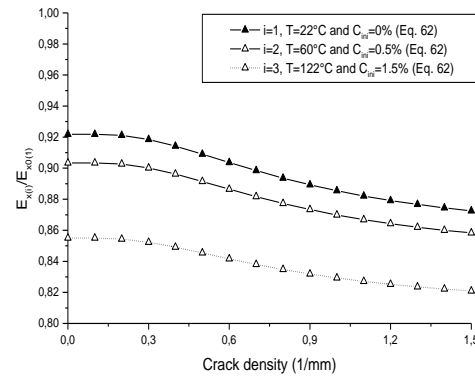


Fig. 12 Hygrothermal effect on the total stiffness degradation due to: (Eq. (62)) transverse cracks and delamination in a  $[0/90_3]_s$  graphite/epoxy (T300/5208)

damaged composite laminates. Additionally, it is observed that the stiffness degradation increases with the rise in crack density and temperature.

The predictions for laminates with only transverse cracks appear to be accurate with experimental data (Ogihara and Takeda 1995) for  $[0/90_m]_s$  laminates at lower crack densities. However, at high crack densities, prediction tend to be inadequate, and delamination consideration proves to be necessary. For laminates in which delamination grows extensively, the modified shear-lag analysis described in the present study has demonstrated the importance of understanding material properties degradation in the failure process. The simultaneous observation of transverse cracks and delamination is necessary for better prediction of Young's modulus reduction.

### 3.2. Analysis of relative stiffness reduction

To analyse the relative stiffness reduction, as explained in section 2.6.1, three sets of environmental conditions are considered. For environmental case 1,  $Top=22^\circ\text{C}$  and  $C=0\%$ . For environmental case 2,  $Top=60^\circ\text{C}$  and  $C=0.5\%$ . For environmental case 3,  $Top=120^\circ\text{C}$  and  $C=1\%$ ,

Table 5 Influence of layers number, environmental parameters, delamination and crack density on total stiffness degradation

	$p$	$q$	$n$ (delamination)	Crack density	$T=22^{\circ}\text{C}$			$T=60^{\circ}\text{C}$		
					$C=0\%$	$C=0,5\%$	$C=1,5\%$	$C=0\%$	$C=0,5\%$	$C=1,5\%$
					Total stiffness degradation rate (%)					
	1	1	0,0	0,0	0,00%	0,00%	0,00%	1,78%	1,79%	1,83%
				0,5	0,83%	0,83%	0,83%	2,54%	2,55%	2,59%
				1,0	1,64%	1,64%	1,64%	3,28%	3,30%	3,33%
				1,5	2,40%	2,40%	2,40%	3,97%	3,98%	4,02%
	1	1	0,8	0,0	4,32%	4,32%	4,32%	5,70%	5,71%	5,74%
				0,5	4,33%	4,33%	4,33%	5,70%	5,72%	5,74%
				1,0	4,40%	4,40%	4,40%	5,77%	5,78%	5,81%
				1,5	4,55%	4,55%	4,55%	5,91%	5,92%	5,95%
	2	2	0,0	0,0	0,00%	0,00%	0,00%	1,78%	1,89%	2,16%
				0,5	0,83%	0,83%	0,83%	2,54%	2,64%	2,90%
				1,0	1,64%	1,64%	1,64%	3,28%	3,38%	3,63%
				1,5	2,40%	2,40%	2,40%	3,97%	4,07%	4,30%
2	2	0,8	0,0	4,32%	4,32%	4,32%	5,70%	5,79%	5,99%	
			0,5	4,33%	4,33%	4,33%	5,70%	5,79%	6,00%	
			1,0	4,40%	4,40%	4,40%	5,77%	5,86%	6,06%	
			1,5	4,55%	4,55%	4,55%	5,91%	5,99%	6,20%	
3	3	0,0	0,0	0,00%	0,00%	0,00%	1,78%	1,93%	2,33%	
			0,5	0,83%	0,83%	0,83%	2,54%	2,68%	3,07%	
			1,0	1,64%	1,64%	1,64%	3,28%	3,42%	3,79%	
			1,5	2,40%	2,40%	2,40%	3,97%	4,10%	4,46%	
3	3	0,8	0,0	4,32%	4,32%	4,32%	5,70%	5,82%	6,13%	
			0,5	4,33%	4,33%	4,33%	5,70%	5,82%	6,13%	
			1,0	4,40%	4,40%	4,40%	5,77%	5,89%	6,20%	
			1,5	4,55%	4,55%	4,55%	5,91%	6,02%	6,33%	

and the chosen simulation time is  $t=100$  h.

The obtained results, as presented in Fig. 9 show that the relative stiffness is reduced by increasing crack density, while temperature and humidity decrease for  $[0/90_3]_s$  graphite/epoxy laminate under transverse cracks only. The reduction rate is approximately 9% to 12%. Conversely, when this laminate is under transverse cracks and delamination (Fig. 10), we observe a small stiffness degradation (reduction rate from 3% to 5% only) due to the laminate quickly reaching the saturation stage. In this case, the hygrothermal effect is more significant even at small crack density.

### 3.3 Analysis of total stiffness reduction

In this section, we undertake a simulation of the comprehensive reduction in stiffness, elucidated in Section 2.6.2. The simulation encompasses the incorporation of reductions attributed to crack density, delamination, moisture content, and fluctuations in temperature.

In Figs. 11-12 the total stiffness is depicted as a function of crack density under various

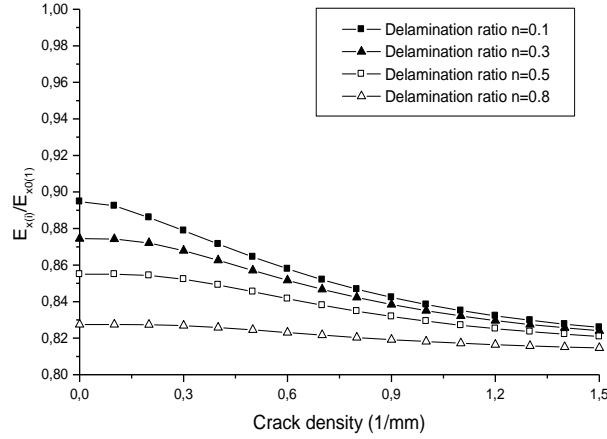


Fig. 13 The total stiffness degradation as a function of crack density for  $[0/90_3]_s$  graphite/epoxy (T300/5208) with different delamination ratio ( $T=122^\circ\text{C}$  and  $C_{mi}=1.5\%$ )

environmental conditions for  $[0/90_3]_s$  graphite/epoxy laminate, considering transverse cracks only (Fig. 11), and transverse cracks in addition to delamination (Fig. 12). Notably the total stiffness exhibits a monotonic reduction with increasing of operational temperature, initial concentration, and crack density. Upon analyzing the hygrothermal impact on cracked laminates relative to uncracked laminates under standard condition (case 1:  $T=22^\circ\text{C}$  and  $C_{mi}=0\%$ ), we note that the most total stiffness degradation is at zero crack density. This mean that the uncracked laminate is more influenced by the temperature and moisture compared to the cracked one.

In order to give an overall view of the obtained results, simulations grouping the following parameters: temperature, humidity, crack density, delamination, number of layers are presented in Table 5. These simulations are conducted on a  $[0^p_p/90^q_q]_s$  laminate, where  $p$  denotes the number of  $0^\circ$  layers,  $q$  the number of  $90^\circ$  layers.

The table reveals several observations:

- The decrease in total stiffness escalates with the augmentation of crack density.
- The reduction of total stiffness is more affected with the appearance of delamination compared to transverse cracking alone ( $n=0$  transverse crack only,  $n=0.8$  transverse crack and delamination).
- The same rate of total stiffness degradation is noted with layers addition (as  $p$  and  $q$  increase) at standard temperature ( $T=22^\circ\text{C}$ ). However, a notable exacerbation in total stiffness reduction is noted with temperature elevation ( $T=60^\circ\text{C}$ ) and the simultaneous increase in the number of layers ( $p=3$  and  $q=3$ ), this phenomenon is attributed to the acceleration of diffusion induced by temperature elevation, exemplifying the thermal activation effects on diffusion processes.

The degradation of total stiffness concerning crack density and various delamination ratios under environmental conditions represented by Case 3 ( $T=122^\circ\text{C}$  and  $C_{mi}=1.5\%$ ) ( $i=3$ ) is illustrated in Fig. 13 for a (T300/5208)  $[0/90_3]_s$  graphite/epoxy laminate. The plot indicates a decline in total stiffness with an increase in delamination ratio ( $n$ ), reaching a point where the effect becomes practically negligible at elevated values of crack density. This suggests that our cracked composite laminate approaches a saturation stage, a phenomenon expedited by rising temperature and moisture concentration levels. Additionally, it is observed that this saturation point is quickly attained under heightened temperature and moisture conditions.

#### 4. Conclusions

The stiffness reduction was predicted using simple analytical models on cross-ply composite laminate including transverse cracks and delamination effect under different environmental conditions by temperature and transient moisture concentration distribution variation in desorption case. The results show a good agreement between prediction models and experimental data. Subsequent to the onset of transverse matrix cracking in composite laminates, notable interlaminar stress concentrations develop at the crack tip, frequently triggering localized delamination at the laminate interface. With the initiation and progression of such local delamination, the stiffness of the composite laminates undergoes significant alteration. Based on the findings presented herein, the following conclusions can be drawn:

- The degradation in stiffness of cracked cross-ply composite laminates featuring transverse cracks and delamination predominantly depend on the augmentation of crack density and thickness ratio.
- The relative stiffness modulus exhibits a consistent decline with an increase in crack density and environmental conditions.
- The total stiffness modulus demonstrates a continuous decrease with rising temperature, humidity levels, and crack density.
- Composite laminates featuring both transverse cracks and delamination are more affected by hygrothermal conditions compared to those with transverse cracks alone.
- Saturation mode is rapidly attained with escalating crack density, delamination ratio, and elevating operational temperature alongside initial moisture content.

Finally, through this theoretical study, we hope that our prediction will serve as a support for future experimental investigations.

#### References

- Adda-Bedia, E.A., Bouazza, M., Tounsi, A., Benzair, A. and Maachou, M. (2008), "Prediction of stiffness degradation in hygrothermal aged [0m/90n] S composite laminates with transverse cracking", *J. Mater. Proc. Technol.*, **199**(1-3), 199-205. <https://doi.org/10.1016/j.jmatprotec.2007.08.002>.
- Barbero, E.J. and Cosso, F.A. (2014), "Determination of material parameters for discrete damage mechanics analysis of carbon-epoxy laminates", *Compos. Part B: Eng.*, **56**, 638-646. <https://doi.org/10.1016/j.compositesb.2013.08.084>.
- Behera, A., Bhoi, N.K., Thawre, M.M., Ballal, A. and Das, D. (2023), "Quantification of hygrothermal aging-induced interfacial debonding of carbon fiber/epoxy composites at nano-to-micrometer length scales", *J. Compos. Mater.*, **57**(30), 4637-4647. <https://doi.org/10.1177/00219983231213912>.
- Behera, A., Vishwakarma, A., Thawre, M.M. and Ballal, A. (2020), "Effect of hygrothermal aging on static behavior of quasi-isotropic CFRP composite laminate", *Compos. Commun.*, **17**, 51-55. <https://doi.org/10.1016/j.coco.2019.11.009>.
- Benkhedda, A. and Tounsi, A. (2008), "Effect of temperature and humidity on transient hygrothermal stresses during moisture desorption in laminated composite plates", *Compos. Struct.*, **82**(4), 629-635. <https://doi.org/10.1016/j.compstruct.2007.04.013>.
- Berthelot, J.M., Leblond, P., El Mahi, A. and Le Corre, J.F. (1996), "Transverse cracking of cross-ply laminates: Part 1. Analysis", *Compos. Part A: Appl. Sci. Manuf.*, **27**(10), 989-1001. [https://doi.org/10.1016/1359-835X\(96\)80002-A](https://doi.org/10.1016/1359-835X(96)80002-A).
- Bouazza, M., Tounsi, A., Benzair, A. and Adda-Bedia, E.A. (2007), "Effect of transverse cracking on stiffness reduction of hygrothermal aged cross-ply laminates", *Mater. Des.*, **28**(4), 1116-1123.

- <https://doi.org/10.1016/j.matdes.2006.02.003>.
- Carraro, P.A., Maragoni, L. and Quaresimin, M. (2019), "Characterisation and analysis of transverse crack-induced delamination in cross-ply composite laminates under fatigue loadings", *Int. J. Fatig.*, **129**, 105217. <https://doi.org/10.1016/j.ijfatigue.2019.105217>.
- Chamis, C.C. (1983), "Simplified composite micromechanics equations for hygral, thermal and mechanical properties", *Ann. Conf. of the Society of the Plastics Industry (SPI) Reinforced Plastics/Composites Inst.*, No. NASA-TM-83320, January.
- Cheng, W. and Cao, Y. (2023), "Investigation of the hygrothermal aging behavior of GFRP laminates used for a marine unmanned aerial vehicle structure", *AIP Adv.*, **13**(4), 045107. <https://doi.org/10.1063/5.0140558>.
- Deepa, A., Padmanabhan, K. and Raghunadh, G. (2016), "Effect of hygrothermal loading on laminate composites", *Ind. J. Sci. Technol.*, **9**(34), 1. <https://10.17485/ijst/2016/v9i34/100979>
- Fernandes, O., Dutta, J. and Pai, Y. (2023), "Effect of various factors and hygrothermal ageing environment on the low velocity impact response of fibre reinforced polymer composites-A comprehensive review". *Cogent Eng.*, **10**(1), 2247228. <https://doi.org/10.1080/23311916.2023.2247228>.
- Fulco, A.P.P., de Medeiros, A.M., Tonatto, M.L.P., Amico, S.C., Talreja, R. and Melo, J.D.D. (2019), "Fatigue damage and fatigue life diagrams of a carbon/epoxy cross ply laminate aged by hygrothermal exposure", *Compos. Part A: Appl. Sci. Manuf.*, **127**, 105628. <https://doi.org/10.1016/j.compositesa.2019.105628>.
- Halpin, J.C. and Tsai, S.W. (1968), "Effects of environmental factors on composite materials", Air Force Materials Lab., AFML-TR.
- Kesba, M.K., Benkhedda, A. and Boukert, B. (2019), "Hygrothermal effect on the moisture absorption in composite laminates with transverse cracks and delamination", *Adv. Aircraft Spacecraft Sci.*, **6**(4), 315-331. <https://doi.org/10.12989/aas.2019.6.4.315>.
- Khodjet-Kesba, M., AddaBedia, E.A., Benkhedda, A. and Boukert, B. (2016), "Prediction of Poisson's ratio degradation in hygrothermal aged and cracked [0m/90n] s composite laminates", *Steel Compos. Struct.*, **21**(1), 57-72. <https://doi.org/10.12989/scs.2016.21.1.057>.
- Khodjet-Kesba, M., Benkhedda, A., Bedia, E.A. and Boukert, B. (2018), "On transverse matrix cracking in composite laminates loaded in flexure under transient hygrothermal conditions", *Struct. Eng. Mech.*, **67**(2), 165-173. <https://doi.org/10.12989/sem.2018.67.2.165>.
- Li, D.H. (2016), "Delamination and transverse crack growth prediction for laminated composite plates and shells", *Comput. Struct.*, **177**, 39-55. <https://doi.org/10.1016/j.compstruc.2016.07.011>.
- Maurice, F.A. (2001), "Engineering composite materials", EMC471, The Pennsylvania State University.
- Rezoug, T., Benkhedda, A., Khodjet-Kesba, M. and Adda, E.A.B. (2011), "Analysis of the composite patches cracked and aged in hygrothermal conditions", *Mecanique Indus.*, **12**(5), 395-398. <https://doi.org/10.1051/meca/2011134>.
- Shen, C.H. and Springer, G.S. (1976), "Moisture absorption and desorption of composite materials", *J. Compos. Mater.*, **10**(1), 2-20.
- Singh, S. and Angra, S. (2019), "Hygrothermal degradation of mechanical properties of nanoclay based stainless steel and glass fibre-epoxy laminate", *J. Phys.: Conf. Ser.*, **1240**(1), 012164. <https://doi.org/10.1088/1742-6596/1240/1/012164>.
- Staab, G. (1999), *Laminar Composite*, Butterworth-Heinemann, London.
- Takeda, N. and Ogihara, S. (1994), "Initiation and growth of delamination from the tips of transverse cracks in CFRP cross-ply laminates", *Compos. Sci. Technol.*, **52**(3), 309-318. [https://doi.org/10.1016/0266-3538\(94\)90166-X](https://doi.org/10.1016/0266-3538(94)90166-X).
- Tsai, S.W. (1988), *Composites Design*, Think Composites, Dayton, Paris, Tokyo.
- van der Meer, F.P. and Sluys, L.J. (2013), "A numerical investigation into the size effect in the transverse crack tension test for mode II delamination", *Compos. Part A: Appl. Sci. Manuf.*, **54**, 145-152. <https://doi.org/10.1016/j.compositesa.2013.07.013>.
- Varun, J.P., Mondal, P. and Mahato, P.K. (2022), "Enhancement of aeroelastic performance of a smart delaminated composite plate under hygrothermal environment", *Compos. Struct.*, **292**, 115662.

- <https://doi.org/10.1016/j.compstruct.2022.115662>.
- Vergnaud, J.M. (1992), *Drying of Polymeric and Solid Materials: Modelling and Industrial Applications*, Springer-Verlag, London.
- Wang, S., Akbolat, M.Ç., Katnam, K.B., Zou, Z., Potluri, P., Sprenger, S. and Taylor, J. (2023), “The effect of hygrothermal ageing on the delamination of Carbon/epoxy laminates with Core-shell rubber nanoparticle and Micro-fibre thermoplastic veil toughening”, *Compos. Part A: Appl. Sci. Manuf.*, **171**, 107576. <https://doi.org/10.1016/j.compositesa.2023.107576>.
- Ye, J., Wu, Y.S., Gao, Y., Gong, C.X., Wang, H., Xu, X.P. and Peng, H.X. (2023), “Hygrothermal aging effects on fiber-metal-laminates with engineered interfaces”, *Compos. Commun.*, **43**, 101721. <https://doi.org/10.1016/j.coco.2023.101721>.
- Zhang, H. and Minnetyan, L. (2006), “Variational analysis of transverse cracking and local delamination in [0m/90n] s laminates”, *Int. J. Solid. Struct.*, **43**(22-23), 7061-7081. <https://doi.org/10.1016/j.ijsolstr.2006.03.004>.
- Zhang, H., Song, Z., Zhang, L., Liu, Z. and Zhu, P. (2023), “Effects of hygrothermal ageing and temperature on the mechanical behavior of aluminum-CFRP hybrid (riveted/bonded) joints”, *Int. J. Adhes. Adhesiv.*, **121**, 103299. <https://doi.org/10.1016/j.ijadhadh.2022.103299>.
- Zhao, L.C., Karimi, S. and Xu, L. (2023), “An experimental investigation of static and fatigue behavior of various adhesive single lap joints under bending loads subjected to hygrothermal and thermal conditions”, *J. Adhes.*, 1-22. <https://doi.org/10.1080/00218464.2023.2270431>.
- Zhu, Y.T. and Xiong, J.J. (2023), “Hygrothermal effect on mechanical behaviours and failure mechanisms of single-lap countersunk-screwed CFRPI-metal joint”, *Mech. Adv. Mater. Struct.*, **30**(17), 3572-3587. <https://doi.org/10.1080/15376494.2022.2079029>.
- Zubillaga, L., Turon, A., Renart, J., Costa, J. and Linde, P. (2015), “An experimental study on matrix crack induced delamination in composite laminates”, *Compos. Struct.*, **127**, 10-17. <https://doi.org/10.1016/j.compstruct.2015.02.077>.